Available online at www.sciencedirect.com
SCIENCE DIRECT
Polymer 46 (2005) 3394–3406
polymer
www.elsevier.com/locate/polymer

Properties of bulk-polymerized thermoplastic polyurethane nanocomposites

Asim Pattanayak, Sadhan C. Jana*

Department of Polymer Engineering, University of Akron, Akron, OH 44325-0301, USA

Received 22 November 2004; received in revised form 21 February 2005; accepted 1 March 2005
Available online 28 March 2005

Abstract

The thermal, rheological, and mechanical properties of bulk-polymerized thermoplastic polyurethane nanocomposites of reactive and non-reactive layered silicate clay were characterized as a function of the state of dispersion of particles. True exfoliated nanocomposites were produced by mixing reactive clay particles with polymer chains carrying residual isocyanate groups. On the other hand, non-reactive clay particles yielded only intercalated composites. Most significant improvement in mechanical properties were obtained when clay particles were fully exfoliated, e.g. 110% increase in tensile modulus, 170% increase in tensile strength, 110% increase in tear strength, 120% increase in fracture toughness, and 40% increase in abrasion resistance over pristine polyurethane with 5 wt% clay. In addition, the terminal dynamic rheological data showed strong dependence on the clay content, indicating substantial hindrance to chain relaxation by tethering clay particles. The peak location and the area under the peak of hydrogen-bonded carbonyl showed two distinct zones of temperature dependence, which indicate additional hydrogen bonding between polymer chains and organic modifier of reactive clays.

Keywords: Reactive clays; Nanocomposites; Exfoliation

1. Introduction

The results reported to date on polyurethane nanocomposites [1–19] list dramatic increases in tensile modulus in all cases, accompanied by increased tensile strength and elongation except for one study [2], where a reduction in tensile modulus was observed. Wei and coworkers [4,7,8,11] prepared first clay-tethered polyurethane nanocomposites in solutions in *N*,*N*′-dimethylformamide (DMF) and observed large enhancements in mechanical and barrier properties. Recently, Zhang et al. [14] reported increases in both tensile strength and elongation at break in bulk polymerized polyurethane–clay nanocomposites, although no tethering between clay particles and polymer chains was inferred; note that the clay particles were intercalated by polyol prior to urethane formation.

Several observations can be made from prior work on polyurethane–clay nanocomposites. First, no consistent bulk polymerization method evolved which can be considered for industrial implementation. Second, there is no consensus that exfoliation of nanoclay is at all possible in this linear polymer system. Third, there is no effort in relating material microstructures to mechanical properties. Recently, we examined two bulk polymerization methods for synthesis of exfoliated TPU nanocomposites of reactive clay [20]. In first method, the clay particles were allowed to react with pre-polymer followed by chain extension with butanediol. In the second, pre-polymer and butanediol underwent chain extension reaction prior to mixing with clay particles. In both methods, polymer chains carried –NCO end groups prior to mixing with clay. However, the second method produced the best results and it was found that both tethering reactions and high shear stress of mixing were necessary for clay particle exfoliation. It was also found that mixing of non-reactive clay with reactive polymer chains and of reactive clay particles with non-reactive polymer chains yielded only microcomposites. The first method, where the clay particles were allowed to react with pre-polymer before chain extension with butanediol, promoted excessive clay–polymer reactions and provided

* Corresponding author. Tel.: +1 330 972 8293; fax: +1 330 258 2339.
E-mail address: janas@uakron.edu (S.C. Jana).

0032-3861/$ - see front matter © 2005 Elsevier Ltd. All rights reserved.
doi:10.1016/j.polymer.2005.03.021

low shear stress of mixing. Consequently, this method yielded only microcomposites.

This paper focuses on characterization of mechanical, thermal, and rheological properties of the clay composites of reactive and non-reactive clay particles produced by the second method. Specifically, we investigated the role of clay–polymer tethering on tensile, fracture, tear, and dynamic rheological properties. A brief review of prior work on thermal and rheological properties of polyurethanes is now in order.

The thermal transitions of segmented polyurethanes is detected by differential scanning calorimetry (DSC) [21–26], although small heat capacity of hard segment phase makes detection of glass transition temperature difficult [27]. Dynamic mechanical thermal analysis (DMTA) is more sensitive than DSC and easily reveals the thermal transitions of both the soft and hard segment phases [22,23,28,29]. At elevated temperatures, say greater than 200 °C, thermoplastic polyurethanes undergo degradation first via decomposition of urethane bonds followed by breakage of the soft segment phase [30,31]. It is anticipated that the presence of nanoparticles can potentially deter thermal degradation of polyurethane chains. Such degradation process can be easily monitored by thermo gravimetric analyses (TGA), mass spectrometry, and Fourier transform infrared (FT-IR) spectrometry [32–34].

FT-IR methods have been used successfully to characterize hydrogen bonds in polyurethanes [35–41]. Two major sources of hydrogen bonds have been identified—those formed by N–H groups of urethanes with ester carbonyl and ether linkages of soft segments and those between N–H groups and carbonyl groups of the urethane segments. The hydrogen bonds show varied degree of stability with temperature as they undergo phase mixing, reorganize, and even dissociate with the increase of temperature [41–45].

Extensive hydrogen bonding also plays profound role in determining rheological properties of polyurethanes. Velankar and Cooper [46] observed that time–temperature superposition was applicable only for TPU with short bock length and attributed the failure of time–temperature superposition to microphase separation. Recently, Yoon and Han [47] observed hysteresis effects arising from microphase separation during isochronal dynamic temperature sweep experiments. Ryan and coworkers [48] attempted to correlate the viscoelastic properties of TPUs with microphase separation transition and found that the complex structure and the intermixing of hard and soft phases at elevated temperature produce complicated rheological behavior. In the present study, TPUs were synthesized with much lower hard segment content, consequently, complicated phase mixing behavior seen by other authors [46,48] was anticipated to have small effects in the current measurements. Nevertheless, the presence of clay particles, especially of those tethered to polymer chains was expected to exert unusual influence on rheological behavior, already seen in other polymer systems [49–51].

2. Experimental

2.1. Materials

Thermoplastic polyurethane (PU) chains were synthesized from a polyetherpolyol (Bayer ARCOL PPG 1025, $M_w \sim 1020$), diphenylmethane diisocyanate (MDI, Bayer Mondur M, $M_w = 250$, melting point 39 °C), and 1,4-butanediol (BD, Fisher Scientific). Fig. 1 lists the chemical structures of these materials. The chain extension reactions between pre-polymer and BD was catalyzed by dibutyltin-laureate catalyst (DABCO 120, Aldrich).

Polyurethane–clay composites were synthesized from two non-reactive and one reactive clay particles. A non-reactive clay, Cloisite®NA+ (clay 1), and a reactive clay, Cloisite®30B (clay 2) were obtained from Southern Clay Products (Gonzales, TX). Cloisite®NA+ is untreated montmorillonite and Cloisite®30B is treated with an organic quaternary ammonium ion $N^+(CH_2CH_2OH)_2(CH_3)T$, where T represents an alkyl group with approximately 65% $C_{18}H_{37}$, 30% $C_{16}H_{33}$, 5% $C_{14}H_{29}$ [52]. The other non-reactive clay (clay 3) was prepared in our laboratory by ion exchange of clay 1 with hexadecylammonium chloride [53]. Clay 3 contained 129 meq of organic per 100 g of clay compared to 92 meq of sodium ions per 100 g of clay in clay 1. This indicates that an excess of hexadecylammonium chloride was present in clay 3. Among these clay particles, only clay 2 was reactive to isocyante groups via $-CH_2CH_2OH$ groups on the quaternary ammonium ions. The scanning electron micrographs (SEM) of treated clay specimens showed particle agglomerates in the size range of 5–20 μm, although individual clay layers were of 1 nm in thickness [54]. The clay particles inherently contained approximately 2 wt% moisture, which was removed by drying in vacuum oven at 80 °C for 24 h.

Table 1 presents molar ratios of various components used in the preparation of polyurethanes with 36% hard segments. In this case, the molar ratio of –NCO and –OH functional groups was maintained at 2:2. In composites of

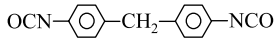

Diphenylmethane diisocyanate (MDI)

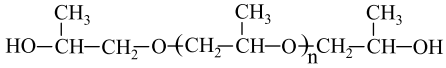

Polyether polyol: poly(propylene glycol)(PPG)

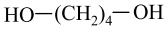

1,4 Butanediol

Fig. 1. Chemical structures of ingredients used in synthesis of polyurethane chains.

Table 1
Mole ratio of various components

Material	Clay content; wt%	MDI/polyol/BD/tallow[a]
Pristine polyurethane	0	2/1/1/0
With clay 1	1	2/1/1/0
	3	2/1/1/0
	5	2/1/1/0
With clay 3	1	2/1/1/0
	3	2/1/1/0
	5	2/1/1/0
With clay 2	1	2/1/0.98/0.02
	3	2/1/0.96/0.04
	5	2/1/0.93/0.07

[a] Organic modifier comes from clay 2.

clay 2, the $-CH_2CH_2OH$ groups of quaternary ammonium ions were taken into consideration while balancing the ratio of –NCO and –OH groups. The basis of such calculation was 90 meq of quaternary ammonium ions per 100 g clay particles. The amounts of treated clay in the composites were maintained at 1, 3, and 5 wt%, which translated, respectively, to 0.76, 2.3, and 3.8 wt% organic-free clay in clay 2 and 0.74, 2.2, and 3.7 wt% organic-free clay in clay 3. In the rest of the text, the clay content will be reported as wt% of treated clay, e.g. clay 2 and clay 3, which contained both organic treatment and organic-free clay particles.

2.2. Nanocomposite preparation

Fig. 2 shows the steps used in the synthesis of nanocomposites. Polyol and BD were dried overnight in vacuum oven at 50 °C; MDI was dried in vacuum oven at room temperature for 1 h. As reflected in Table 1, MDI and polyol were mixed in molar ratio of 2:1 and allowed to react for 2 h at a temperature of 80 °C under nitrogen flow to produce pre-polymer (step 1, Fig. 2) with number (M_n) and weight average (M_w) molecular weights of ~2800 and ~4300, respectively.

Chain extension between pre-polymer and butanediol was carried out at 80 °C for 6 min in a batch mixer, Brabender Plasticoder (Model EPL 7752) catalyzed by 2.3×10^{-7} mol/cm^3 of dibutyltinlaureate catalyst (step 2, Fig. 2). Note that chain-extended polymer chains used in clay composites carried residual –NCO groups. Such chains will be referred to as 'reactive polymer chains'. The clay particles were mixed with reactive polymer chains at a temperature of 80 °C for another 9 min (step 3, Fig. 2). This allowed time for possible reactions between the –NCO groups of polymer chains and the $-CH_2CH_2OH$ groups in particles of clay 2. For comparison purposes, pristine thermoplastic polyurethane with no residual –NCO end groups was first prepared and then mixed with 5 wt% clay 2 in Brabender Plastocoder at 80 °C for 9 min to prepare the 'control' material. Note that the control material was prepared under the same conditions of viscosity and temperature as the composite of reactive polymer chains and clay 2 as described in Fig. 2.

2.3. Characterization

The state of intercalation/exfoliation behavior of clay structures was studied by wide-angle X-ray diffraction (WAXD) method and transmission electron microscopy (TEM). The WAXD patterns were generated using Rigaku X-ray diffractometer (wavelength, $\lambda = 1.54$ Å). TEM images of microtomed specimens were taken at 120 kV using TACNAI-12 TEM device.

The thermal properties were evaluated by differential scanning calorimetry (DSC) using Dupont DSC (model DSC-2910) under nitrogen atmosphere at a scanning rate of 20 °C/min over a temperature range of −50 to 250 °C. The composite materials were also analyzed thermo-gravimetrically by Dupont TGA 2950 at a scanning rate of 20 °C/min from room temperature to 800 °C under nitrogen atmosphere.

Fourier-transform infrared spectroscopy (FT-IR) was used to characterize hydrogen bonding. A Perkin Elmer (Model 16PC) FT-IR with a resolution of 4 cm^{-1} was used. The specimens were cast into films on KBr discs from a solution in THF and dried thoroughly to remove the traces of THF.

A rotational rheometer (ARES, TA Instruments) was used for rheological measurements under oscillatory mode with a 25 mm diameter parallel plate fixture. Dynamic storage modulus (G'), loss modulus (G''), and complex viscosity ($|\eta^*|$) were measured as functions of angular frequency (ω) ranging from 0.1 to 100 rad/s and a fixed strain of 0.04. All measurements were conducted under nitrogen flow. A temperature of 150 °C was chosen for such

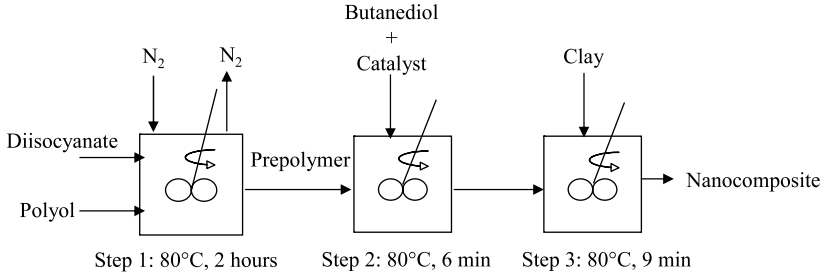

Fig. 2. Method of synthesis of nanocomposites.

measurements with the expectation that a majority of the hydrogen bonds with the clay particles would be broken at such temperature and only the effects of clay–polymer tethering would be captured.

Dynamic mechanical thermal analysis (DMTA) was carried out by Rheometric Scientific DMTA V device with single point bending of the 2 mm thick strip at a frequency of 1 Hz and a heating rate of 4 °C/min from −50 to 150 °C. The maximum of tan δ values was used to determine the glass transition temperature (T_g).

Tensile tests were performed at room temperature following ASTM D 638 type V method using Instron 5567 machine. The crosshead speed was 50 mm/min. For each specimen, five measurements were taken and average values of tensile strength, modulus, and strain were calculated.

Tear strength was determined by using Instron (model 5567) machine, with cross head speed of 50 mm/min at room temperature. Sample specimens of dimensions 120×15×2 mm^3 with a 4 mm deep perpendicular cut were used.

Plane-stress fracture toughness tests were conducted by in-house horizontal tensile testing machine with a crosshead speed of 1.166 mm/min. The rectangular specimens of dimensions 100×16×2 mm^3 with about 4 mm deep sharp notch at the middle of the specimens were stretched under load. The crack-tip region was observed at a magnification of 100 using a camera. The onset of crack propagation was noted and the fracture toughness was calculated from the following equation [55,56]:

$$K_c = \sqrt{3.94\left(\frac{2w}{\pi a}\right)\tan\left(\frac{\pi a}{2w}\right)}\sqrt{a}\left(\frac{F}{[w-a]b}\right) \quad (1)$$

where, K_c is the plane–stress fracture toughness, w is the sample width, a is the notch length, F is the force on the sample when crack propagation begins, and b is the sample thickness.

The abrasion resistance was determined by Zwick Abrasion Tester 6102, which is similar to DIN 53 516, according to ASTM D5963 with the following parameters: force 2.5 N, sample height 2 mm, speed of the drum 40 rpm. The sample specimen was cylindrical in shape with 16 mm of diameter. The weight loss by the sample in each cycle was measured and reported as a loss of volume from an average of three samples.

3. Results and discussion

3.1. Morphology

The WAXD patterns presented in Fig. 3 were taken for composites with 5 wt% clay. A broad diffraction peak at $2\theta = 3.75°$ (d-spacing ~2.3 nm) is seen for composites of clay 1, while sharp peaks at $2\theta = 3$ and 5.2° (d-spacing ~2.9 and 1.7 nm, respectively) are seen for clay 3. In these cases,

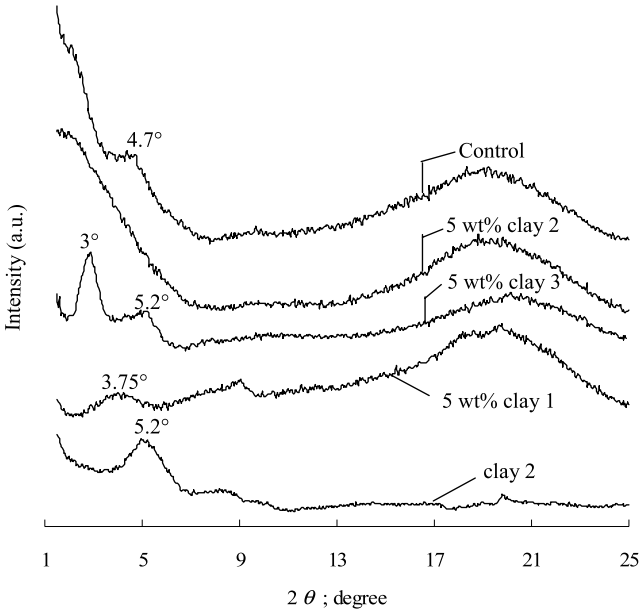

Fig. 3. WAXD patterns of nanocomposites. The pattern for clay 2 is presented as a reference.

the residual clay peaks at $2\theta = 3.75$ and 3° indicate partial intercalation of clay layers by the polymer chains, while peaks at $2\theta = 5.2°$ indicate residual treated clay particles in the composite. The same observations were made for composites of 1 and 3 wt% clay 1 and clay 3 particles [20]. The composite of clay 2 with 5 wt% clay shows no distinguishable peak for $2\theta > 1.5°$ in WAXD patterns (Fig. 3) indicating that the separation between two adjacent clay layers was at least 6 nm. The TEM image (Fig. 4(a)) of the composite supports this and shows that individual clay layers were well-dispersed in the polymer. The composites of 1 and 3 wt% clay 2, however, contained mostly intercalated tactoids. In view of this, a true nanocomposite was produced only in the case of 5 wt% clay 2.

The control material of 5 wt% clay 2, produced under similar conditions of viscosity and temperature as the nanocomposite of 5 wt% clay 2, was a microcomposite as evident from WAXD pattern in Fig. 3 and TEM image in Fig. 4(b). A sharp peak at $2\theta = 4.7°$ (d-spacing ~1.9 nm) in Fig. 3 is close to the original clay 2 peak at $2\theta = 5.2°$. This contrast in the degree of dispersion of clay 2 particles endorses that clay–polymer reactions were necessary to obtain exfoliated TPU nanocomposites as established in our earlier work [20].

3.2. FT-IR spectra

Table 2 summarizes the ratio of areas under various characteristic peaks e.g. free carbonyl at 1725 cm^{-1} (A_{FCO}), hydrogen bonded carbonyl at 1701 cm^{-1} (A_{HCO}), free –NH at 3337 cm^{-1} and hydrogen bonded –NH at 3290–3307 cm^{-1} (A_{NH}) with respect to the area under the –CH stretching peak (A_{CH}) between 2866 and 2972 cm^{-1}. The

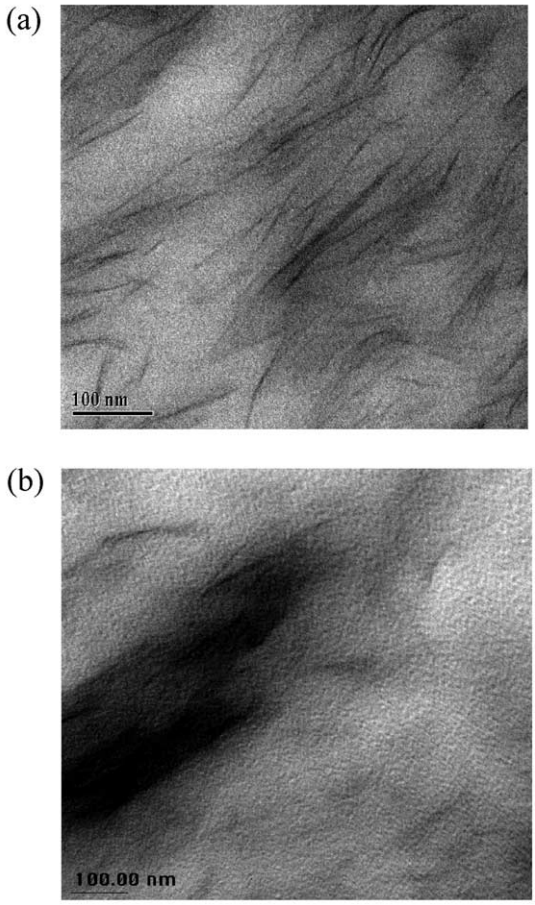

Fig. 4. TEM images of 5 wt% clay composites (a) clay 2, (b) control.

value of A_{CH} was used as an internal standard. It is noted in Table 2 that the total area under carbonyl peak A_{CO} is slightly higher for clay composites than for pristine PU, although the fraction of hydrogen-bonded carbonyls reduced with clay content except in the case of 5 wt% clay 2. In addition, A_{NH}/A_{CH} ratio is much smaller in clay composites. In view of these, the following can be concluded: (1) the fraction of urethane –NH groups hydrogen-bonded to ether linkages of soft segments and to carbonyl groups of hard segments reduced in presence of clay particles, which may have strong impact on mechanical properties. (2) The excess hydrogen-bonded carbonyl groups in the case of 5 wt% clay 2 may have originated from hydrogen bonding between urethane carbonyls and residual $–CH_2CH_2OH$ groups of the quaternary ammonium ions. The control material, however, showed values of A_{NH}/A_{CH} and A_{HCO}/A_{CH} ratios closer to those of PU. We observed in our earlier report [20] that hydrogen bonding did not facilitate clay particle dispersion to nanoscale.

Table 2
Ratio of the area under the peak of hydrogen-bonded –NH (A_{NH}), total C=O (A_{CO}), and –CH stretching (A_{CH}) of FT-IR spectra and the ratio of area under the peak of hydrogen bonded C=O (A_{HCO}) and free C=O (A_{FCO}) groups

Material	A_{NH}/A_{CH}	A_{CO}/A_{CH}	A_{HCO}/A_{FCO}
PU	0.41	0.54	1.04
With clay 1			
1 wt%	0.29	0.59	0.81
3 wt%	0.29	0.60	0.79
5 wt%	0.29	0.60	0.77
With clay 2			
1 wt%	0.30	0.63	0.87
3 wt%	0.31	0.64	0.89
5 wt%	0.33	0.65	0.98
With clay 3			
1 wt%	0.26	0.63	0.81
3 wt%	0.25	0.63	0.80
5 wt%	0.25	0.63	0.78
Control with 5 wt% clay 2	0.39	0.54	0.91

Let us now investigate the thermal stability of these hydrogen bonds. For this purpose, the PU-clay nanocomposites were heated between two KBr discs in FT-IR to a maximum temperature of 190 °C. No unusual behavior [43] was noticed in the FT-IR diagram at 190 °C; therefore, it was assumed that decomposition of urethane linkage did not take place at this temperature. Figs. 5 and 6 show the variations of absorption due to N–H stretching and –C=O stretching respectively with temperature. Note that in each case only the data for pristine polyurethane and composite of 5 wt% clay 2 are compared. The following observations can be made from inspection of Figs. 5 and 6. (1) The sharp peak respectively at 3337 cm^{-1} (Fig. 5) and 1702 cm^{-1}

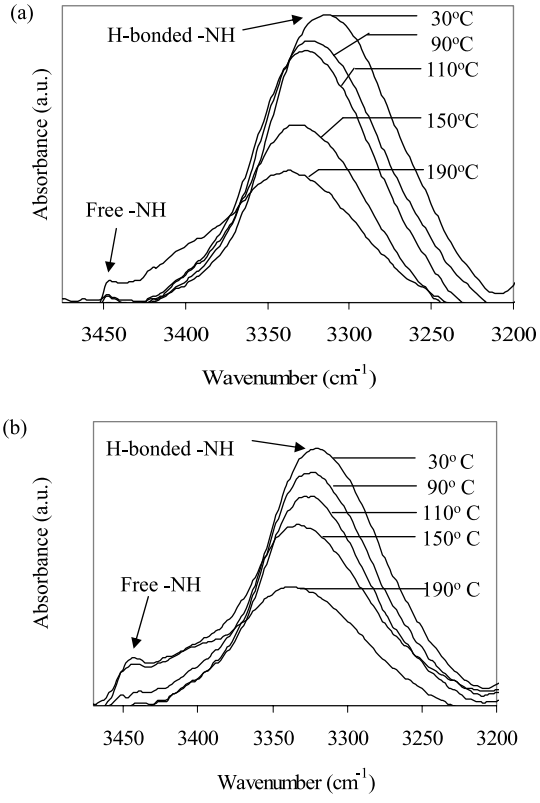

Fig. 5. FT-IR spectra of N–H stretching region at various temperatures: (a) pristine PU and (b) composite of 5 wt% clay 2.

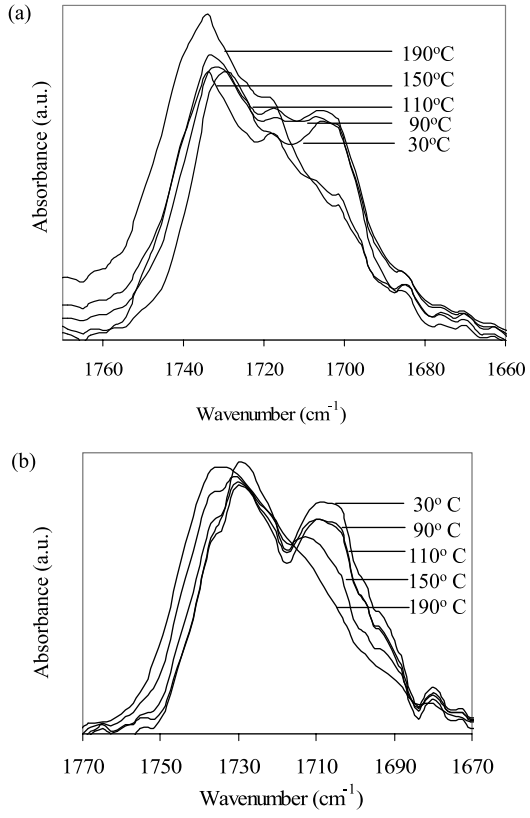

Fig. 6. FT-IR spectra of –C=O stretching region at various temperatures (a) pristine PU and (b) composite of 5 wt% clay 2.

(Fig. 6) indicate that most of the N–H groups and –C=O groups remained hydrogen bonded at 30 °C. (2) The intensity of hydrogen bonded N–H peaks decreased and the intensity of free N–H bands (at 3337 cm^{-1}) increased with temperature; similarly, the absorption peak intensities of free carbonyl groups increased at the expense of hydrogen bonded carbonyl groups. (3) The peaks of both hydrogen bonded N–H and carbonyl absorption shifted to higher frequency with the increase of temperatures (Fig. 7).

The data of Figs. 5 and 6 can be recast by plotting the area under the peaks of hydrogen bonded –NH and carbonyl groups as function of temperature, as shown in Fig. 8. The ratio A_{NH}/A_{CH} decreased almost linearly with temperature and the nature of clay had almost no effect on the slope (Fig. 8(a)). The values of A_{HCO}/A_{CH} also decreased linearly with temperature, but with two slopes as observed by previous investigators [43]: (1) in the range 30–90 °C for clay 1 and 30–110 °C in the case of clay 2 and pristine polyurethane and (2) at temperatures greater than 90 °C, Fig. 8(b). Such changes in slopes are consistent with the literature and have been attributed to differences in the values of extinction coefficients [43]. Nevertheless, an appreciable value of A_{HCO}/A_{CH} at higher temperature in the case of clay 2 in Fig. 8(b) can be ascribed to higher thermal stability of hydrogen bonds between urethane carbonyls and $–CH_2CH_2OH$ groups of quaternary ammonium ions. Note that high temperature

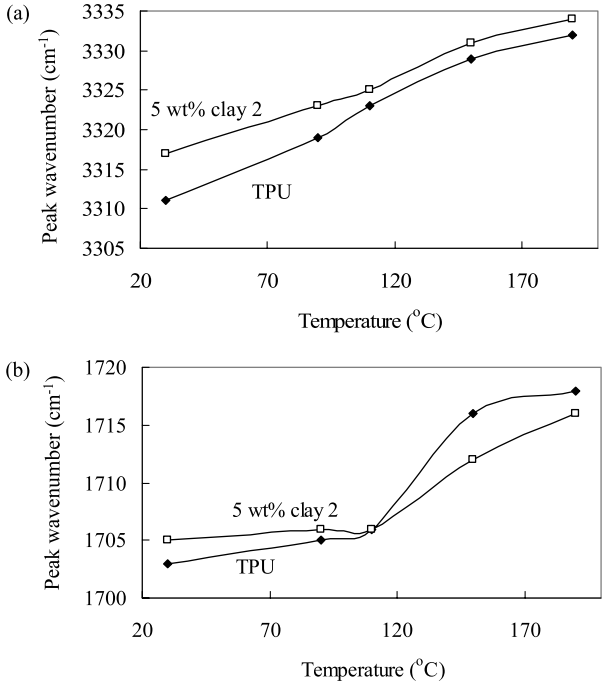

Fig. 7. The change of hydrogen bonded peak wavenumber with temperature of IR spectra. (a) –NH stretching and (b) –C=O stretching.

values of A_{HCO}/A_{CH} ratio for clay 1 and clay 2 are similar to pristine polyurethane.

3.3. Tensile properties

Typical stress–strain diagrams of polyurethane and

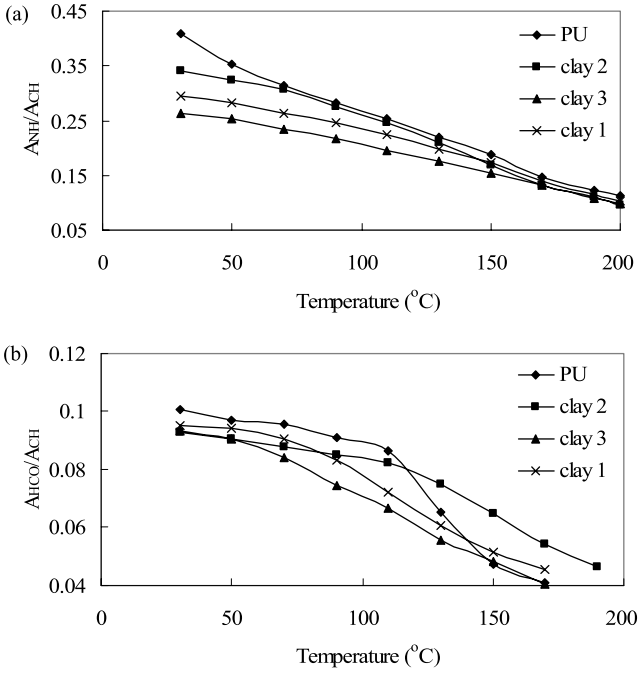

Fig. 8. Effect of temperature on hydrogen bonding: (a) –N–H stretching and (b) –C=O stretching.

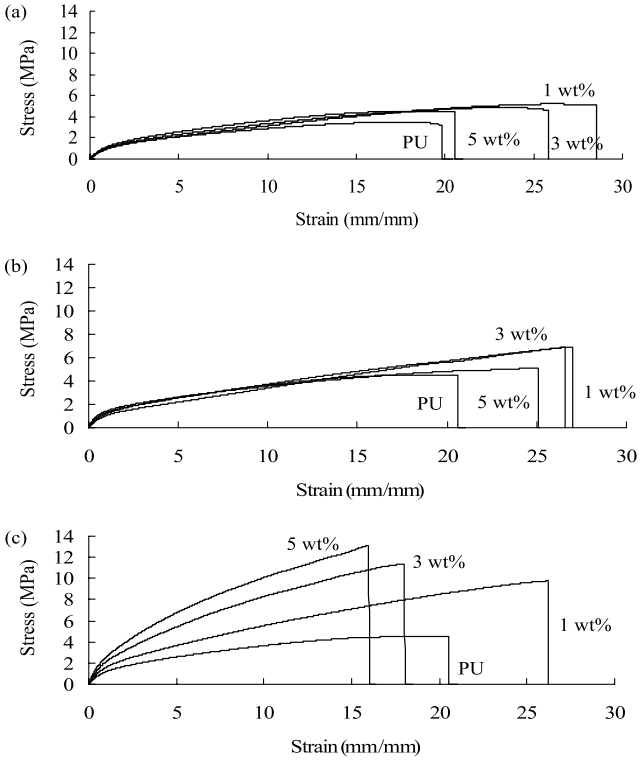

Fig. 9. Stress–strain diagrams of PU and nanocomposites with (a) clay 1, (b) clay 3, and (c) clay 2.

polyurethane composites of three types of clay are shown in Fig. 9. The modulus and tensile strength increased for all three clay loadings in composites of clay 2. However, these properties remained insensitive to clay content in composite of clay 1, though the composite of 1 wt% clay 3 showed improvements in both tensile stress and strain at break. In the nanocomposite of 5 wt% clay 2, the modulus and tensile strength increased by 110 and 170%, respectively, over pristine PU (Table 3). Note that such improvement can be

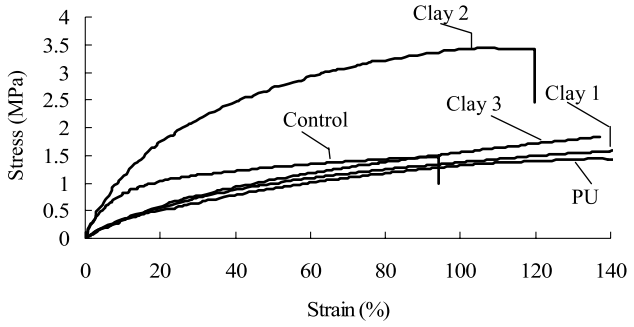

Fig. 10. Tear stress vs. strain diagram of composites with 5 wt% clay.

attributed to clay–polymer tethering as well as hydrogen bonding between clay particles and the polymer.

Let us now discuss if hydrogen bonding had much impact on the tensile strength. As already seen in Table 2, the values of A_{NH}/A_{CH} and A_{HCO}/A_{CH} ratios for the control material are similar to that of composite of clay 2, although the value of tensile strength reported in Table 3 ($\sim$3.4 MPa) is much smaller than that of the composite of clay 2 ($\sim$12.8 MPa) with 5 wt% clay content. This indicates that hydrogen bonding did not contribute significantly to the tensile strength of the clay composites. The values of tensile modulus, on the other hand, were dominated by the clay particles.

The strain at break did not improve as much in the presence of clay 2 particles. This can be attributed to restrictions on the mobility of polymer chains during stretching by the tethering clay particles.

3.4. Tear strength

Table 4 shows the values of tensile tear stress, strain, modulus, and energy for break of composites and pristine PU. Fig. 10 represents typical stress–strain diagrams of specimen during tear tests. As in tensile tests, the nanocomposite of 5 wt% clay 2 shows a maximum value

Table 3
Tensile properties of polyurethane nanocomposites

Material	Modulus (MPa) ± standard deviation	Maximum stress (MPa) ± standard deviation	Strain at break (%)
PU	1.4 ± 0.1	4.7 ± 0.04	2100
With clay 1			
1 wt%	1.1 ± 0.05	5.2 ± 0.1	2800
3 wt%	1.3 ± 0.06	4.9 ± 0.2	2500
5 wt%	1.4 ± 0.04	3.6 ± 0.1	2000
With clay 2			
1 wt%	1.7 ± 0.15	9.7 ± 0.2	2500
3 wt%	2.3 ± 0.11	11.2 ± 0.3	2000
5 wt%	3.0 ± 0.06	12.8 ± 0.6	1800
With clay 3			
1 wt%	1.5 ± 0.1	7.2 ± 0.7	2850
3 wt%	1.9 ± 0.05	7.6 ± 0.1	2700
5 wt%	2.4 ± 0.3	5.1 ± 0.1	2500
Control with 5 wt% clay 2	3.2 ± 0.29	3.4 ± 0.09	1100

Table 4
Tear properties of polyurethane nanocomposites

Material	Modulus at 100% strain (MPa) ± standard deviation	Stress at break (MPa) ± standard deviation	Strain at break (%) ± standard deviation	Energy for break (J) ± standard deviation
PU	1.3 ± 0.02	1.5 ± 0.06	155 ± 16	2.85 ± 0.3
With clay 1				
1 wt%	1.3 ± 0.04	1.6 ± 0.08	190 ± 35	3.6 ± 0.9
3 wt%	1.4 ± 0.05	1.7 ± 0.05	180 ± 12	3.6 ± 0.4
5 wt%	1.6 ± 0.04	2.1 ± 0.04	190 ± 25	4 ± 0.8
With clay 2				
1 wt%	2.1 ± 0.06	2.2 ± 0.08	115 ± 10	3.04 ± 0.07
3 wt%	2.8 ± 0.07	2.8 ± 0.10	105 ± 8	3.4 ± 0.3
5 wt%	3.2 ± 0.03	3.2 ± 0.10	105 ± 12	4 ± 0.5
With clay 3				
1 wt%	1.5 ± 0.01	1.8 ± 0.09	200 ± 25	3.4 ± 0.9
3 wt%	1.8 ± 0.08	2.0 ± 0.06	184 ± 17	3.7 ± 0.06
5 wt%	2.0 ± 0.04	2.1 ± 0.04	174 ± 8	4.2 ± 0.4
Control with 5 wt% clay 2	3.0 ± 0.02	1.9 ± 0.08	95 ± 10	2.7 ± 0.3

of stress at break, which is 110% higher than that of pristine PU. The resistance to growth of fracture, measured in terms of stress at break indicates that clay tethering and uniform dispersion of clay 2 particles inhibited stress concentration and delayed crack propagation. The composite materials of clay 1, clay 3, and control material on the other hand, performed poorly due to microdispersed clay particles and almost no clay–polymer tethering reactions. The tear modulus of the composites also increased with the increase of clay loading and it reached maximum value in the case of 5 wt% clay 2 nanocomposites. As in the case of tensile elongation, nanocomposites of clay 2 did not show any improvement in strain at break. However, the energy required to break increased with the increase of clay loading (Table 4).

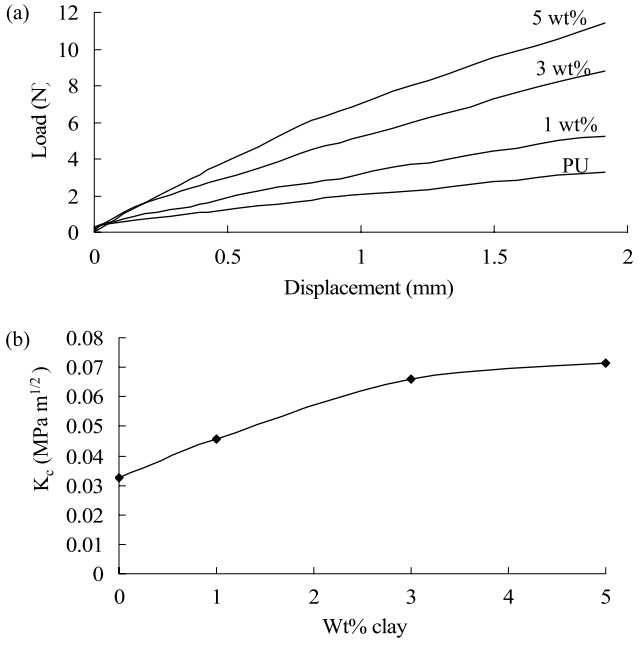

Fig. 11. Fracture toughness of nanocomposites with clay 2 (a) load–displacement diagram and (b) K_c vs. clay wt%.

3.5. Fracture toughness

The load–displacement curves during fracture are shown in Fig. 11(a) for nancomposites of clay 2. The best-fit straight line for each case is presented instead of the raw data points. The values of plane–stress fracture toughness (K_c) of the nanocomposites were calculated based on Eq. (1) and the results are presented in Table 5. The values of K_c increased with the increase of clay 2 content (Fig. 11(b))—approximately 120% increase over TPU is observed with 5 wt% clay 2, while the control material and the composites of 5 wt% clay 1 showed lower values. The composite of 5 wt% clay 3 showed some improvement over pristine TPU, but not as much as the nanocomposite of clay 2.

3.6. Abrasion resistance

The loss of materials of pristine polyurethane and clay-filled polyurethane composites are presented in Table 6, which indicates that the abrasion resistance of composites of clay 1 and clay 3 was almost the same as pristine polyurethane. However, the abrasion resistance of nanocomposites of clay 2 improved significantly and the volume loss reduced by 40% in the nanocomposite of 5 wt% clay 2.

Table 5
Fracture toughness test results of polyurethane nanocomposites

Material	K_c MPa(m)$^{1/2}$ ± standard deviation
PU	0.032 ± 0.002
With clay 2	
1 wt%	0.045 ± 0.002
3 wt%	0.066 ± 0.007
5 wt%	0.071 ± 0.008
With clay 3	
5 wt%	0.058 ± 0.003
With clay 1	
5 wt%	0.031 ± 0.002
Control with clay 2	
5 wt%	0.029 ± 0.010

Table 6
Abrasion test results

Material	Volume loss (cm^3/g) ± standard deviation
PU	0.079 ± 0.008
Composites with clay 1	
1 wt%	0.081 ± 0.006
3 wt%	0.080 ± 0.009
5 wt%	0.078 ± 0.004
Composites with clay 2	
1 wt%	0.080 ± 0.007
3 wt%	0.059 ± 0.004
5 wt%	0.046 ± 0.001
Composites with clay 3	
1 wt%	0.086 ± 0.004
3 wt%	0.080 ± 0.002
5 wt%	0.073 ± 0.001
Control with clay 2	
5 wt%	0.074 ± 0.005

This enhancement of abrasion resistance was the result of polymer–clay tethering, which was absent in control material and in composites of clay 1 and clay 3. The SEM images of abraded surface of pristine PU and nanocomposite of 5 wt% clay 2 are shown in Fig. 12. It is seen that the abraded surface of the nanocomposite appears much smoother than the pristine polyurethane, which indicate that nanodispersed clay particles dictated the local failure mode and consequently the loss of materials.

3.7. Thermal properties

The glass transition temperature (T_g) and melting point (T_m) of polyurethane nanocomposites are given in Table 7. The soft segments of the pre-polymer and pristine PU showed T_g of −28 and −6 °C, respectively. It is seen in Table 7 that glass transition temperature of soft-segment phase did not change much due to the presence clay particles. However, this is not surprising as the soft

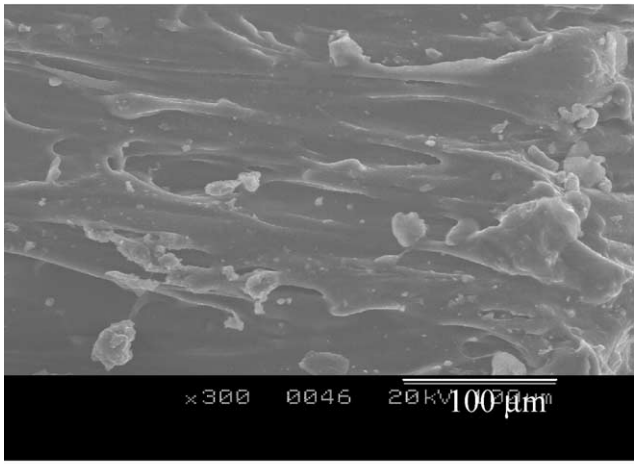

Fig. 12. SEM images of abraded surface of (a) PU and (b) nanocomposite of 5 wt% clay 2.

Table 7
Thermal properties of polyurethane nanocomposites

Material	T_g (°C)	T_m (°C)	T_1 (°C)[a]	T_2 (°C)[b]	Residue (%)[c]
PU	−6	140	290	367	1.62
With clay 1					
1 wt%	−3	138	287	352	1.90
3 wt%	−2	140	292	364	3.93
5 wt%	−2	146	293	381	5.26
With clay 2					
1 wt%	−3	143	286	370	3.02
3 wt%	−2	141	288	386	6.46
5 wt%	−1	146	290	390	9.43
With clay 3					
1 wt%	−2	141	285	377	2.79
3 wt%	−2	142	286	385	7.49
5 wt%	−4	147	286	388	9.53
Control with 5 wt% clay 2	−2	138	279	390	9.53

[a] Temperature at 5% weight loss obtained from TGA curve.
[b] Peak temperature obtained from DTGA curve.
[c] Residue at 800 °C obtained from TGA curve.

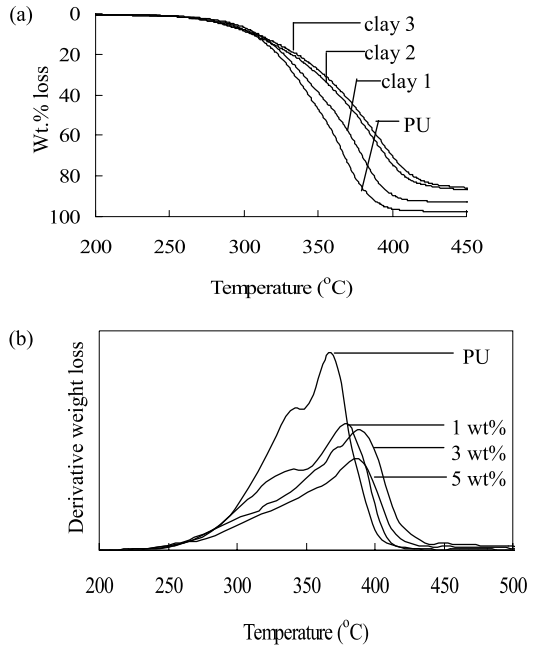

Fig. 13. Thermo-gravimetric analysis (a) weight loss and (b) derivative weight loss of nanocomposites of clay 2.

segments of chain-extended polymers were already formed before clay particle addition. The melting transitions corresponding to hard-segment phases were relatively small and were not affected by the clay particles. The value of enthalpy associated with melting in each case was also small, indicating that only small fraction of urethane linkages formed phase separated domains.

The thermal stability of pristine PU and its composites of clay 1, clay 3, and clay 2 were investigated by thermo-gravimetric analyzer (TGA). The degradation behavior of the composites is shown in Fig. 13. The first degradation temperatures (T_1), i.e. the temperatures at 5% weight loss of composites, with the exception of the control material were in the same neighborhood of pure PU (Fig. 13(a) and Table 7). Note that the first degradation is mostly dominated by the degradation of organic modifier present in the clay. The derivative of the weight loss curves gave distinct degradation temperature peak (T_2) (Fig. 13(b) and Table 7), where the effect of clay particles is clearly seen. The T_2 values of composites of clay 2, clay 3, and even control material were about 20 °C higher than those of pristine PU and composite of clay 1. This result indicates that clay–polymer reactions had almost no effect on thermal degradation behavior.

3.8. Dynamic mechanical thermal analysis (DMTA)

The tan δ peaks are attributed to the backbone motion of the soft-segment phase and produce glass transition temperature. The T_g values obtained from Fig. 14 are shown in Table 8. The tan δ peaks of composites of clay 2 (Fig. 14(a)) shifted towards higher T_g values whereas, for other two types of composites, e.g. of clay 1 and clay 3 and

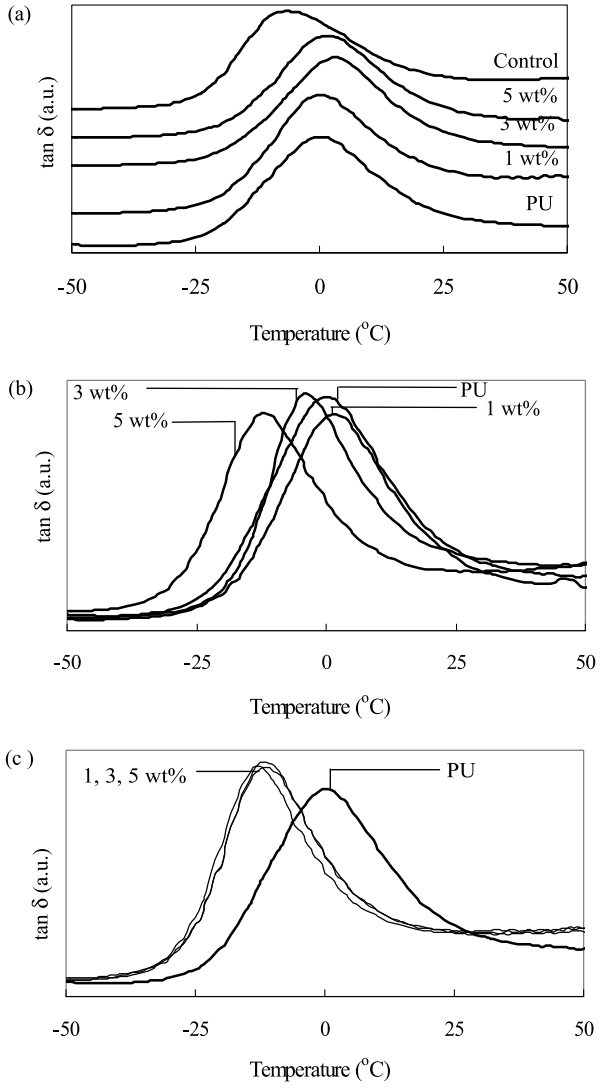

Fig. 14. tan δ peaks from DMTA test of composites with (a) clay 2 (b) clay 3, and (c) clay 1.

the control material, the shifting of peaks was observed towards lower T_g with the increase of clay loading (Fig. 14(b) and (c)). The increase of T_g values in clay 2 nanocomposites was the result of clay particle tethering to polymer chains, which was absent in other two composites. This statement is also supported by storage modulus data given in Table 8. The storage moduli of all three composites of clay 2 were much higher than for other composites and pristine PU (Fig. 15). At −50 °C, the storage modulus (G') of nanocomposites with 5 wt% clay 2 was 1.7 fold higher than that of pristine PU, while composites of clay 1 provided modulus lower than pristine PU. Also note that the T_g values of the soft segment phases of nanocomposites, measured in DMTA test, were different from those measured by DSC. The T_g values of composites of clay 2 were higher, whereas the values for composites of non-reactive clays and control material were lower than the values obtained from DSC experiment. This can be due to differences in the rate of

Table 8
Dyanamic mechanical properties of polyurethane nanocomposites

Material	$T_{g,soft}$[a] (°C)	G' (Pa)×10^9 at −50 °C
PU	0.8	1.58
With clay 1		
1 wt%	−12	1.38
3 wt%	−10	1.46
5 wt%	−10	1.50
With clay 2		
1 wt%	1.5	2.36
3 wt%	3	2.47
5 wt%	3.4	2.62
With clay 3		
1 wt%	−10	2.01
3 wt%	−4	2.09
5 wt%	1	2.37
Control with 5 wt% clay 2	−6	2.22

[a] Glass transition temperature of soft segment from the peaks of tan δ vs, frequency curves.

heating, e.g. 20 °C/min in DSC vs. 4 °C/min in DMTA and the mode of experiments, e.g. static vs. dynamic respectively in DSC and DMTA.

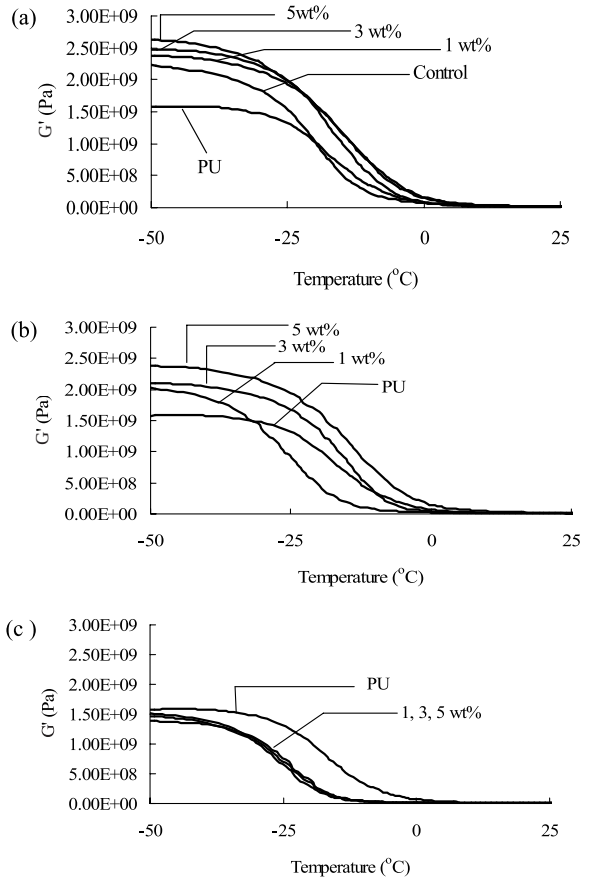

Fig. 15. Storage modulus (G') from DMTA test of composites of (a) clay 2 (b) clay 3, and (c) clay 1.

3.9. Rheological behavior

The linear viscoelastic properties of pristine PU and its composites with 5 wt% clay 1, clay 2, and clay 3 were measured as presented in Fig. 16. The storage modulus (G') (Fig. 16(a)) increased monotonously with the increase of frequency in all cases, but the composites of clay 2 and control material show much higher values of modulus at lower frequencies than pristine PU and other composites. A lower value of G' in the case of clay 1 can be attributed to micro-scale clay particles, with negligible clay–polymer interactions, while relatively higher values in the case of clay 3 came possibly from clay–polymer interactions via intercalating polymer chains, as evident from the shifting of X-ray peaks in Fig. 3.

The G' vs. ω curves show a plateau-like behavior (Fig. 16(a)) at low values of ω in the case of nanocomposite of clay 2, similar to other clay–polymer nanocomposites [49–51]. This resulted from strong polymer–particle interactions due to clay–polymer tethering, uniform nanoscale dispersion, and much larger surface area of clay particles

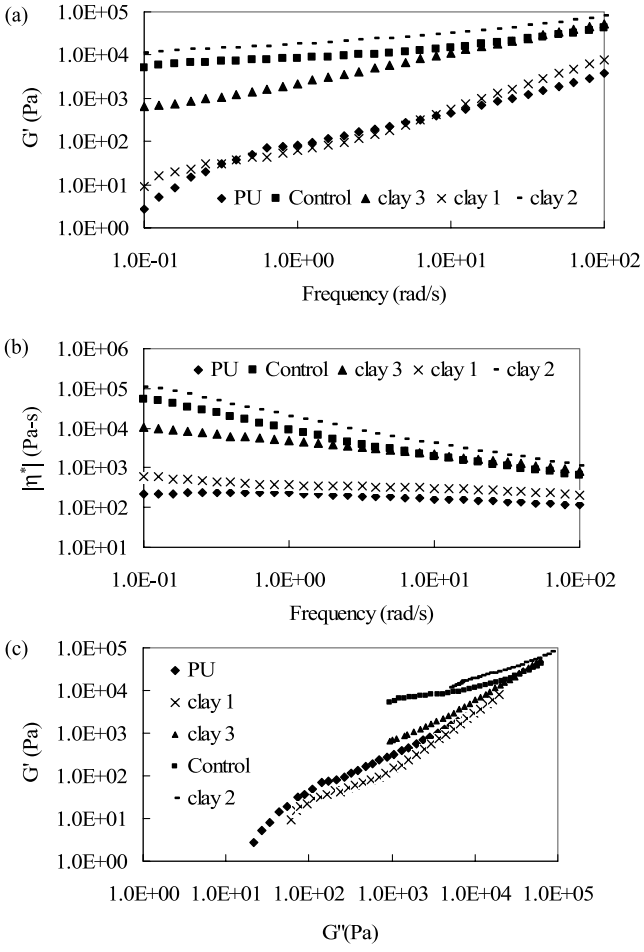

Fig. 16. Dynamic rheological properties of pristine PU and its composites with 5 wt% clay (a) storage modulus (G'), (b) complex viscosity (η^*) and (c) G' vs. G''. All measurements were carried out with 4% strain at a temperature of 150 °C.

Table 9
The values of indices in the relationships, $G' \sim \omega^a$; $G'' \sim \omega^b$; $G' \sim (G'')^\alpha$

Material	a	b	α
PU	1.9	1.0	1.8
Clay 1			
1 wt%	1.2	0.8	1.4
3 wt%	1.07	0.87	1.2
5 wt%	0.95	0.8	1.2
Clay 2			
1 wt%	0.56	0.68	0.8
3 wt%	0.49	0.61	0.8
5 wt%	0.24	0.57	0.4
Clay 3			
1 wt%	0.91	0.82	1.1
3 wt%	0.74	0.75	1.0
5 wt%	0.71	0.68	1.0
Control with 5 wt% clay 2	1.05	0.83	1.3

exposed to polymer chains. The dependence of G' and G'' on ω in the terminal zone was calculated for each composite using the following relationships: $G' \sim \omega^a$; $G'' \sim \omega^b$; $G' \sim (G'')^\alpha$. It is seen in Table 9 that the values of a and b reduce significantly due to the presence of clay. The measured values of a ($\sim$1.9) and b ($\sim$1.0) for pristine polyurethane are close to the ideal homopolymer values of respectively 2.0 and 1.0. The largest reduction ($a \sim 0.24$ and $b \sim 0.57$) is seen in the nanocomposite of 5 wt% clay 2, indicating that tethering clay particles significantly retarded the motion of polymer chains.

Fig. 16(b) shows plots of complex viscosity ($|\eta^*|$) versus angular frequency (ω) for various materials. The complex viscosity increased substantially with the increase of clay content and the values were higher in the case of clay 2, again due to clay tethered polymer chains. This enhancement can be explained on the basis of resistance to flow and deformation of the molten polymer chains imposed by tethered clay particles.

A plot of G' vs. G'' can also represent the dynamics of end-tethered polyurethane chains (Fig. 16(c)). The slopes (α) of low frequency region (<10 rad/s) were estimated and reported in Table 9. It was found that the values of α reduced from its value of 1.83 for pristine PU with the increase of clay loading. The reduction was largest in the case of nanocomposites of clay 2. Comparatively higher value of α in the case of control material confirms that polymer–clay tethering reactions were the primary reason behind much reduced values of α in nanocomposites of clay 2.

4. Conclusions

The materials prepared from reactive polymer chains and reactive clay provided the scope for substantial increase in modulus and tensile strength, thermal stability, tear strength, fracture toughness, and abrasion resistance with low clay loading than the common, physical blends of polymer and clay particles, as in the control material. The true nanocomposite offered the best improvement in properties. The dynamic rheological properties showed that nanoclay–polymer chain tethering also posed significant restrictions on polymer chain relaxation. The study also concluded that additional hydrogen bonding between nanodispersed clay particles and urethane carbonyls had insignificant contribution to tensile strength values.

Acknowledgements

Partial financial support was obtained from National Science Foundation in the form of CAREER Award to SCJ.

References

[1] Wang Z, Pinnavaia TJ. Chem Mater 1998;10:3769.
[2] Zilg C, Thomann R, Muelhaupt R, Finter J. Adv Mater 1999;11:49.
[3] Petrovic ZS, Javni I, Waddon A, Banhegyi G. J Appl Polym Sci 2000; 76:133.
[4] Chen TK, Tien YI, Wei KH. Polymer 2000;41:1345.
[5] Xu R, Manias E, Snyder AJ, Runt J. Macromolecules 2001;34:337.
[6] Ma J, Zhang S, Qi Z. J Appl Polym Sci 2001;82:1444.
[7] Tien YI, Wei KH. Macromolecules 2001;34:9045.
[8] Tien YI, Wei KH. Polymer 2001;42:3213.
[9] Hu Y, Song L, Xu J, Yang L, Chen Z, Fan W. Colloid Polym Sci 2001; 279:819.
[10] Yao KJ, Song M, Hourston DJ, Luo DZ. Polymer 2002;43:1017.
[11] Tien YI, Wei KH. J Appl Polym Sci 2002;86:1741.
[12] Chang JH, An YU. J Polym Sci, Part B: Polym Phys 2002;40:670.
[13] Tortora M, Gorrasi G, Vittoria V, Galli G, Ritrovati S, Chiellini E. Polymer 2002;43:6147.
[14] Zhang X, Xu R, Wu Z, Zhou C. Polym Int 2003;52:790.
[15] Song M, Hourston DJ, Yao KJ, Tay JKH, Ansarifar MA. J Appl Polym Sci 2003;90:3239.
[16] Mishra JK, Kim I, Ha CS. Macromol Rapid Commun 2003;24:671.
[17] Chen X, Wu L, Zhou S, You B. Polym Int 2003;790.
[18] Rhoney I, Brown S, Hudson NE, Pethrik RA. J Appl Polym Sci 2003; 91:1335.
[19] Osman MA, Mittal V, Morbidelli M, Suter UW. Macromolecules 2003;36:9851.
[20] Pattanayak A, Jana SC. Polymer 2005; in press, doi 10.1016/j.polymer.2005.02.081.
[21] Sung CSP, Schneider NS. Macromolecules 1975;8:68.
[22] Miller JA, Lin SB, Hwang KKS, Wu KS, Gibson PE, Cooper SL. Macromolecules 1985;18:32.
[23] Wang CB, Cooper SL. Macromolecules 1983;16:775.
[24] Seymour RW, Cooper SL. Macromolecules 1973;6:48.
[25] Koberstein JT, Russel TP. Macromolecules 1986;19:714.
[26] Leung LM, Koberstein JT. Macromolecules 1986;19:706.
[27] Chen TK, Chui JY, Sheih TS. Macromolecules 1997;30:5068.
[28] Ryan AJ, Stanford JL, Still RH. Polymer 1991;32:1426.
[29] Ng HN, Allegrezza AE, Seymour RW, Cooper SL. Polymer 1973;14: 255.
[30] Yang WP, Macosko CW, Wellinghoff ST. Polymer 1986;27:1235.
[31] Petrovic ZS, Zavargo Z, Flynn JH, Macknight WJ. J Appl Polym Sci 1994;51:1087.
[32] Lage LG, Kawano Y. J Appl Polym Sci 2001;79:910.
[33] Chang CT, Shen WS, Chiu YS. Polym Degrad Stab 1995;49:353.
[34] Suhara F, Kutty SKN, Nando GB. Polym Degrad Stab 1998;61:9.
[35] Lee HS, Wang YK, Hsu SL. Macromolecules 1987;20:2089.

[36] Lee HS, Wang YK, Macknight WJ, Hsu SL. Macromolecules 1988; 21:270.
[37] Tao HJ, Meuse CW, Yang X, Macknight WJ, Hsu SL. Macromolecules 1994;27:7146.
[38] Meuse CW, Yang X, Yang D, Hsu SL. Macromolecules 1992;25:925.
[39] Camargo RE, Macosko CW, Tirrell MV, Wellinghoff ST. Polym Eng Sci 1982;22:719.
[40] Coleman MM, Lee KH, Skrovanek DJ, Hu J, Painter PC. Macromolecules 1986;19:2149.
[41] Coleman MM, Lee KH, Skrovanek DJ, Painter PC. Macromolecules 1986;19:2149.
[42] Seymour RW, Estes GW, Cooper SL. Macromolecules 1970;3: 1579.
[43] Srichatrapimuk VW, Cooper SL. J Macromol Sci Phys 1978;B15:267.
[44] Senich GA, Macknight WJ. Macromolecules 1980;13:106.
[45] Klempner D, Frisch KC (ed.) Polymer alloys: Blends, Blocks, Grafts and Interpenetrating Networks, Polymer Science and Technology, Vol 10, New York: Plenum Press; 1977. p.287.
[46] Velankar S, Cooper SL. Macromolecules 1998;31:9181.
[47] Yoon PJ, Han CD. Macromolecules 2000;33:2171.
[48] Ryan AJ, Macosko CW, Bras W. Macromolecules 1992;25:6277.
[49] Krishnamoorti R, Giannelis EP. Macromolecules 1997;30:4097.
[50] Ayyer RK, Leonov AI. Rheol Acta 2004;43:283.
[51] Lim YT, Park OO. Rheol Acta 2001;40:220.
[52] http://www.nanoclay.com/data/30B.htm
[53] Park JH, Jana SC. Macromolecules 2003;36:2758.
[54] Grim RH. Clay mineralogy. New York: McGraw-Hill; 1953.
[55] Hertzberg RW. Deformation and fracture mechanics of engineering materials. 3rd ed. New York: Wiley; 1989.
[56] Balard RL, Sailer RA, Larson B, Soucek MD. J Coat Technol 2001; 73:107.